DALTON

Linear trinuclear oximato-bridged complexes $Mn^{III,IV}M^{II}Mn^{III,IV}$ (M = Zn, Cu or Mn): synthesis, structure, redox behaviour and magnetism ‡

Frank Birkelbach,[a] Thomas Weyhermüller,[a] Marek Lengen,[b] Michael Gerdan,[b] Alfred X. Trautwein,[b] Karl Wieghardt[a] and Phalguni Chaudhuri*,†,[a]

[a] *Max-Planck-Institut für Strahlenchemie, Stiftstrasse 34-36, D-45470 Mülheim an der Ruhr, Germany*
[b] *Institut für Physik, Medizinische Universität, D-23538 Lübeck, Germany*

Six trinuclear linear complexes $[LMn^{III}\{\mu\text{-}(niox)_3M^{II}\}Mn^{III}L]^{2+}$ **1**–**3** and $[LMn^{IV}\{\mu\text{-}(niox)_3M^{II}\}Mn^{IV}L]^{4+}$ **4**–**6** where M represents either Zn (**1** and **4**), Cu (**2** and **5**) or Mn (**3** and **6**), containing three cyclohexane-1,2-dione dioximate dianions (niox) as bridging ligands and 1,4,7-trimethyl-1,4,7-triazacyclononane (L) as the capping ligand for the terminal manganese-(III) or -(IV) ions, have been synthesized. They have been characterized by elemental analysis, IR, UV/VIS and EPR spectroscopy, cyclic voltammetry, and by variable-temperature (2–295 K) magnetic susceptibility and isothermal magnetization measurements. The trinuclear complexes are quasi-isostructural with the terminal manganese ions in a distorted octahedral environment, MnN_3O_3, and the divalent metal ions M are six-co-ordinate with a $M^{II}N_6$ chromophore. The molecular structure of the compound $[LMn^{IV}\{\mu\text{-}(niox)_3Zn^{II}\}Mn^{IV}L][ClO_4]_4$ **4** has been established by X-ray diffraction. The structure consists of tris(nioximato)-bridged $Mn^{IV}Zn^{II}Mn^{IV}$ tetracations and non-co-ordinated perchlorate anions, with an intramolecular $Mn^{IV}\cdots Mn^{IV}$ distance of 6.97 Å. A crystal structure determination of $Mn^{IV}Cu^{II}Mn^{IV}$ **5** was not up to normal crystallographic standards. Nevertheless, the atom connectivities together with the heterotrinuclear nature with Mn^{IV} as the terminal ions are clear. The cyclic voltammograms of **1**–**6** reveal two reversible and two quasi-reversible one-electron redox processes, $Mn^{III}M^{II}Mn^{III} \overset{Ox_1}{\rightleftharpoons} Mn^{IV}M^{II}Mn^{III} \overset{Ox_2}{\rightleftharpoons} Mn^{IV}M^{II}Mn^{IV}$ and $Mn^{III}M^{II}Mn^{III} \overset{Red_1}{\rightleftharpoons} Mn^{II}M^{II}Mn^{III} \overset{Red_2}{\rightleftharpoons} Mn^{II}M^{II}Mn^{II}$. The central divalent metal ion is redox inactive. Analyses of susceptibility data showed the occurrence of intramolecular ferro- and antiferro-magnetic exchange interactions. There are indeed two different coupling constants, J_a operating between the adjacent metal centres and J_t between the terminal centres, separated by a large distance of ≈7 Å. The effect of J_t on the splitting pattern has been shown by the variability of the ground states. That the assumption commonly made of no coupling between the terminal ions in trinuclear linear complexes may lead to a wrong spin ground state has been conclusively demonstrated. An analysis of the interacting magnetic orbitals in complexes containing three metal centres is presented.

We have been interested in tailor-made synthesis of heteropolynuclear clathrochelates, *i.e.* multicyclic ligand systems that completely encapsulate a metal ion, with varying metal d^n configurations by using suitably designed metal oximates and the metal-containing capping agent ML as building blocks, where L represents the macrocyclic amine 1,4,7-trimethyl-1,4,7-triazacyclononane.[1] In this connection we have demonstrated experimentally the phenomenon of spin ground-state variability for linear trinuclear complexes of the type $M_AM_BM_A$, in which two different coupling constants $J = J_{AB} = J_{BA}$ and J_{AA} are operative; the terminal metal centres M_A, separated by a large distance of ≈7 Å, are antiferromagnetically coupled ($-J_{AA} \approx 5$–$20\ cm^{-1}$). In a recent publication[2] we have reported tris(dimethylglyoximato)-bridged $Mn^{IV}M^{II}Mn^{IV}$ complexes, where M = Mn^{II}, Ni^{II}, Cu^{II} or Zn^{II}, but without any structural characterization, because of the unavailability of X-ray-quality crystals. As very little is known about heterometallic complexes containing Mn^{IV}, we have extended our studies and explored the possibility of obtaining good-quality crystals by changing dimethylglyoxime (H_2dmg) to cyclohexane-1,2-dione dioxime (nioxime, abbreviated as 'H_2niox').

Herein we report the synthesis, electrochemical, magnetic and spectroscopic properties of six niox-bridged complexes $[LMn^{III}\{\mu\text{-}(niox)_3M^{II}\}Mn^{III}L][ClO_4]_2$ where M = Zn^{II} **1**, Cu^{II} **2** or Mn^{II} **3** and $[LMn^{IV}\{\mu\text{-}(niox)_3M^{II}\}Mn^{IV}L][ClO_4]_4$ where M = Zn^{II} **4**, Cu^{II} **5** or Mn^{II} **6**, together with the crystal structure of $Mn^{IV}Zn^{II}Mn^{IV}$ **4** and the atom connectivities for **5**, $Mn^{IV}Cu^{II}Mn^{IV}$, as found by a mediocre-quality X-ray diffraction analysis. Throughout this paper the compounds are denoted by the metal centres only for the sake of clarity.

Experimental

Materials

Reagent or analytical grade materials were obtained from commercial suppliers and used without further purification, except those for electrochemical measurements. The macrocycle 1,4,7-trimethyl-1,4,7-triazacyclononane ($L = C_9H_{21}N_3$) was prepared as described previously.[3] 'Manganese(III) acetate' with the formula $[Mn_3O(MeCO_2)_7]\cdot 3H_2O$ was prepared according to the literature method.[4]

Physical measurements

A Perkin-Elmer Lambda 9 spectrophotometer was used to record UV/VIS spectra. Fourier-transform infrared spectroscopy on KBr pellets was performed on a Perkin-Elmer 1720X FTIR instrument. Cyclic voltammetric experiments were made with a Princeton Applied Research model 173 potentio-

† E-Mail: Chaudh@mpi-muelheim.mpg.de
‡ *Non-SI unit employed:* $\mu_B \approx 9.27 \times 10^{-24}\ J\ T^{-1}$.

stat-galvanostat driven by a model 175 universal programmer, and details of the experimental procedure have been described earlier.[5] Variable-temperature (2–295 K) magnetic susceptibility measurements were carried out on a Quantum Design MPMS SQUID magnetometer with an applied field of 1 T. Diamagnetic corrections were made using Pascal's constants. The X-band EPR spectra of the polycrystalline material either as a solid or in solution were recorded at various temperatures between 3 and 100 K with a Bruker ER 200 D-SRC spectrometer equipped with a standard TE 102 cavity, an Oxford Instruments liquid-helium continuous-flow cryostat, a NMR gaussmeter, a frequency meter, and a data-acquisition system (own development).

Synthesis of the compounds

The trimetallic manganese(III) complexes $[LMn^{III}\{\mu\text{-}(niox)_3Zn^{II}\}Mn^{III}L][ClO_4]_2$ **1**, $[LMn^{III}\{\mu\text{-}(niox)_3Cu^{II}\}Mn^{III}L][ClO_4]_2$ **2** and $[LMn^{III}\{\mu\text{-}(niox)_3Mn^{II}\}Mn^{III}L][ClO_4]_2$ **3** have been synthesized by a similar protocol.

'Manganese(III) acetate' (0.27 g, 1 mmol) was added to a deaerated solution of 1,4,7-trimethyl-1,4,7-triazacyclononane (0.17 g, 1 mmol) in methanol (40 cm^3) under vigorous stirring. The red-brown solution, obtained after 0.5 h of stirring, was charged with solid samples of either $Zn(MeCO_2)_2\cdot 2H_2O$ (0.11 g, 0.5 mmol) **1**, $Cu(MeCO_2)_2\cdot H_2O$ (0.10 g, 0.5 mmol) **2** or $Mn(MeCO_2)_2\cdot 4H_2O$ (0.12 g, 0.5 mmol) **3**, nioxime (0.21 g, 1.5 mmol) and triethylamine (1 cm^3). The red-brown solution was refluxed for 0.5 h and the hot solution was filtered to remove any solid particles. A neutral solution of triethylammonium toluene-*p*-sulfonate (0.5 g) in methanol and Pr^iOH (5 cm^3) were added to the deep brown solution, which upon standing at ambient temperature yielded within 1–2 d black needles of **1***, **2*** or **3*** as toluene-*p*-sulfonate salts. The crystals were filtered off, washed with cold ethanol and air-dried.

Complex **1***: yield = 0.30 g (45%) (Found: C, 46.1; H, 6.3; Mn, 8.6; N, 12.6. $C_{50}H_{80}Mn_2N_{12}O_{12}S_2Zn\cdot 2H_2O$ requires C, 45.61; H, 6.43; Mn, 8.34; N, 12.77%); IR(KBr, $\tilde{\nu}_{max}/cm^{-1}$) 1597m (CN), 1181s, 1097s (NO), ≈1200s (br) (SO_3); UV/VIS (MeOH) λ_{max}/nm (ε/dm^3 mol^{-1} cm^{-1}) 293 (sh) (29 900), 307 (30 400), 420 (sh) (4600), 540 (sh) (1010) and 1350 (35).

Complex **2***: yield = 0.37 g (56%) (Found: C, 45.8; H, 6.4; Mn, 8.2; N, 12.7. $C_{50}H_{80}CuMn_2N_{12}O_{12}S_2\cdot 2H_2O$ requires C, 45.67; H, 6.44; Mn, 8.36; N, 12.78%); IR(KBr, $\tilde{\nu}_{max}/cm^{-1}$) 1580m (br) (CN), 1193s (br), 1070s (NO), ≈1200s (br) (SO_3); UV/VIS (MeOH) λ_{max}/nm (ε/dm^3 mol^{-1} cm^{-1}) 277 (35 000), ≈450 (sh) (4200) and 580 (sh) (1610).

Complex **3***: yield = 0.30 g (45%) (Found: C, 46.1; H, 6.4; Mn, 12.6; N, 12.9. $C_{50}H_{80}Mn_3N_{12}O_{12}\cdot 2H_2O$ requires C, 45.98; H, 6.48; Mn, 12.62; N, 12.87%); IR(KBr, $\tilde{\nu}_{max}/cm^{-1}$) 1582m (CN), 1180s, 1090s (NO), ≈1200s (br) (SO_3); UV/VIS (MeOH) λ_{max}/nm (ε/dm^3 mol^{-1} cm^{-1}) 288 (28 300), 319 (sh) (24 500) and 527 (1860).

The perchlorate salts **1**–**3** were obtained in more than 80% yield by adding a solution of $NaClO_4\cdot H_2O$ in methanol, instead of toluene-*p*-sulfonate, to the above-mentioned red-brown solution. They are practically insoluble in common organic solvents.

$[LMn^{IV}\{\mu\text{-}(niox)_3M^{II}\}Mn^{IV}L][ClO_4]_4$ (M^{II} = Zn 4, Cu 5 or Mn 6). As complexes **4**–**6** were prepared in a very similar way, a representative method only is described. An argon-scrubbed suspension of **1**, **2** or **3** (0.26 g, ≈0.2 mmol) in MeCN (40 cm^3) was stirred with $NOBF_4$ (47 mg, ≈0.4 mmol) for an hour under argon. Within a few minutes an appreciable darkening of the suspension occurred and gradually a clear dark solution was obtained. The nearly black solution was filtered in the air to remove any solid particles. After addition of dry $NaClO_4$ (0.2 g) dissolved in a small amount of MeCN and on cooling at 4 °C, dark microcrystals were collected within an hour by filtration, washing with cold acetonitrile and air-dried. Yield: 50–60%. X-Ray-quality crystals were obtained after 1–2 d directly from the reacting solutions without any addition of $NaClO_4$.

Complex **4** (Found: C, 32.5; H, 5.1; Mn, 8.0; N, 12.6; Zn, 4.6; ClO_4, 30.0. $C_{36}H_{66}Cl_4Mn_2N_{12}O_{22}Zn$ requires C, 32.36; H, 4.98; Mn, 8.22; N, 12.58; Zn, 4.89; ClO_4, 29.77%); IR(KBr, $\tilde{\nu}_{max}/cm^{-1}$) 1621w (CN); UV/VIS (MeOH) λ_{max}/nm (ε/dm^3 mol^{-1} cm^{-1}) 277 (33 750), 320 (sh) (25 200) and 408 (25 760).

Complex **5** (Found: C, 32.4; H, 5.0; Cu, 5.1; Mn, 8.4; N, 12.5; ClO_4, 30.0. $C_{36}H_{66}Cl_4CuMn_2N_{12}O_{22}$ requires C, 32.41; H, 4.99; Cu, 4.76; Mn, 8.24; N, 12.60; ClO_4, 29.82%). IR(KBr, $\tilde{\nu}_{max}/cm^{-1}$) 1609w (sh) (CN); UV/VIS (MeOH) λ_{max}/nm (ε/dm^3 mol^{-1} cm^{-1}) 278 (36 700), 420 (sh) (9200), 660 (sh) (2600) and 1068 (908).

Complex **6** (Found: C, 32.8; H, 5.0; Mn, 12.6; N, 12.4; ClO_4, 30.8. $C_{36}H_{66}Cl_4Mn_3N_{12}O_{22}$ requires C, 32.61; H, 5.02; Mn, 12.43; N, 12.68; ClO_4, 30.00%). IR(KBr, $\tilde{\nu}_{max}/cm^{-1}$) 1600 (sh) (CN); UV/VIS (MeOH) λ_{max}/nm (ε/dm^3 mol^{-1} cm^{-1}) 283 (30 700), 390 (sh) (10 300), 520 (sh) (3660), 695 (sh) (1470) and 1090 (1143).

CAUTION: although no problems were encountered in this work, perchlorate salts of metal complexes with organic ligands are potentially explosive and should thus be prepared in small quantities and handled with care.

Crystallography

X-Ray diffraction data for complex **4** were collected at 173 K with a Siemens P4 diffractometer using graphite-monochromatized Mo-Kα radiation (λ = 0.710 73 Å). Crystallographic data and structure refinement parameters are given in Table 2. Data were collected by the 2θ–ω scan method ($3 \leqslant 2\theta \leqslant 50°$). Three standard reflections monitored every 100 showed no significant variations. The data were corrected for absorption[6] and Lorentz-polarization effects.

The structure was solved by direct methods and subsequent Fourier-difference techniques, and refined anisotropically, by full-matrix least squares, on F^2 (program SHELXTL PLUS).[7] Hydrogen atoms were included at calculated positions with $U = 0.08$ Å^2 in the last cycle of refinement.

Owing to the high degree of orientational disorder of perchlorate anions and the solvent acetonitrile, the *R* factor is not very satisfactory, 0.096. The solvent molecule MeCN was refined with a site occupation of 0.5.

CCDC reference number 186/731.

Results and Discussion

The red-brown solution obtained from 'manganese(III) acetate' and the cyclic amine (L) in methanol affords the dinuclear complex cation $[Mn^{III}_2(\mu\text{-}O)(\mu\text{-}MeCO_2)_2L_2]^{2+}$, as described previously.[8] The cation reacts with the $[M^{II}(niox)_3]^{4-}$ ion, prepared *in situ*, and yields upon addition of perchlorate or toluene-*p*-sulfonate as counter anion dark brown crystals of $[L_2Mn^{III}_2(niox)_3M^{II}]X_2$. A basic medium needed for deprotonation of the O···H···O groups present in the metal(II) oximate molecules is provided by the added triethylamine. Presumably the dianionic $[M^{II}(niox)_2]^{2-}$ species produced in this way acts as a template for the formation of the bicycle by subsequent addition of an dianionic $niox^{2-}$ ligand; these three oxime ligands now orient in such a way that various metal-containing capping agents, *i.e.* a co-ordinatively unsaturated metal–ligand fragment ML, generate linear trinuclear complexes of the type $M_tM_cM_t$, where the subscript 't' stands for terminal and 'c' for central. It is interesting that although the complexes $Mn^{III}Ni^{II}Mn^{III}$ and $Mn^{IV}Ni^{II}Mn^{IV}$ could be prepared for dimethylglyoxime[2] as the bridging dioxime ligand, all attempts to isolate such species with nioxime were unsuccessful, presumably due to the completely insoluble character of $[Ni(Hniox)_2]$ under the reaction conditions.

Table 1 Electrochemical data for complexes **1***–**3*** in V *vs.* normal hydrogen electrode

		$E_{\frac{1}{2}}$			
Complex	$E_{p,ox}$	Ox_2	Ox_1	Red_1	Red_2
1* $Mn^{III}Zn^{II}Mn^{III}$	—	0.65 (r)	0.43 (r)	−0.31 (qr)	−0.62 (qr)
2* $Mn^{III}Cu^{II}Mn^{III}$	—	0.72 (r)	0.43 (r)	−0.34 (qr)	−0.63 (ir)
3* $Mn^{III}Mn^{II}Mn^{III}$	+1.27	0.74 (r)	0.43 (r)	−0.21 (r)	−0.56 (qr)

r = Reversible, qr = quasi-reversible, ir = irreversible.

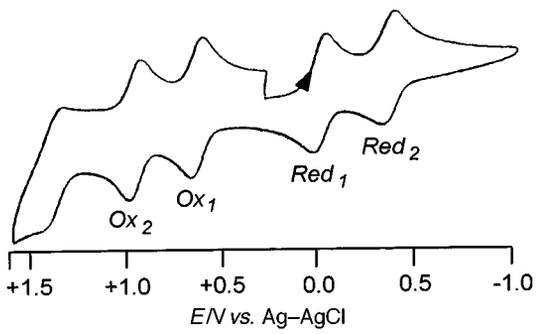

Fig. 1 Cyclic voltammogram of complex **3*** in MeCN at a scan rate of 0.2 V s^{-1} (0.1 mol dm^{-3} NBu_4PF_6, platinum working electrode, ambient temperature)

The trinuclear complexes $Mn^{III}Zn^{II}Mn^{III}$ **1**, $Mn^{III}Cu^{II}Mn^{III}$ **2** and $Mn^{III}Mn^{II}Mn^{III}$ **3** are amenable to oxidation, as is evident from the electrochemical experiments, and yield $Mn^{IV}M^{II}Mn^{IV}$ complexes (M^{II} = Zn **4**, Cu **5** or Mn **6**) when oxidized in acetonitrile with NO^+ cation.

The optical spectra of complexes **1**–**6** have been measured in the 200–1400 nm wavelength range. On the basis of high absorption coefficients and the relative sharpness of the bands, most bands can be ascribed to charge-transfer transitions within the ligands or metal-to-ligand charge transfer (MLCT). The bands at 1068 nm for **5**, 1090 nm for **6** and 1350 nm for **1** are thought to be due to ligand-field (d–d) transitions.

The infrared spectra of complexes **1**–**6** have in common peaks attributable to the presence of 1,4,7-trimethyl-1,4,7-triazacyclononane and unco-ordinated perchlorate [1090–1100s, $\nu_{asym}(ClO_4)$; 620–625m cm^{-1}, $\delta_{asym}(ClO_4)$]. A very strong broad band at ≈1200 cm^{-1} for the sulfonate groups is observed. The medium-strong bands at 1180–1193 cm^{-1} for **1***–**3*** are assignable to the NO stretching vibration.[9] Interestingly, the corresponding bands for **4**–**6** are very weak. The second NO infrared absorption could not be observed for the perchlorate salts because of superposition of the strong band originating from the perchlorate anion. However, for the toluene-*p*-sulfonate salts the second NO stretch has been identified unambiguously at 1097 cm^{-1} for **1***, 1070 cm^{-1} for **2*** and 1090 cm^{-1} for **3***. The ν(CN) vibrations of complexes **1***–**3*** containing trivalent manganese ions are situated at significantly lower frequency, 1580–1597 cm^{-1}, than those for the corresponding tetravalent manganese ions, 1600–1621w cm^{-1}.

Electrochemistry

The cyclic voltammogram of $Mn^{III}Mn^{II}Mn^{III}$ **3*** at ambient temperature in MeCN containing tetra-*n*-butylammonium hexafluorophosphate as supporting electrolyte at a platinum-button working electrode at a scan rate of 200 mV s^{-1} is shown in Fig. 1. Electrochemical data for complexes **1***–**3*** are summarized in Table 1. Two consecutive reversible oxidation steps in the potential range 0.0 to 1.0 V *vs.* Ag–AgCl are detected for **1***–**3*** corresponding to the electrochemical oxidation processes $Mn^{III}M^{II}Mn^{III} \overset{Ox_1}{\rightleftharpoons} Mn^{IV}M^{II}Mn^{III} \overset{Ox_2}{\rightleftharpoons} Mn^{IV}M^{II}Mn^{IV}$. That two reversible transfers of one electron per metal centre occur is evident from the adherence to the standard criteria.[10] The reversible character of $E_{\frac{1}{2}}(Ox_1)$ and $E_{\frac{1}{2}}(Ox_2)$ precludes any significant structural rearrangement during the redox processes; *i.e.* all three species have the same structure in solution and apparently can be described by the solid-state structure as determined by X-ray diffraction of $Mn^{IV}ZnMn^{IV}$ **4** and $Mn^{IV}CuMn^{IV}$ **5**.

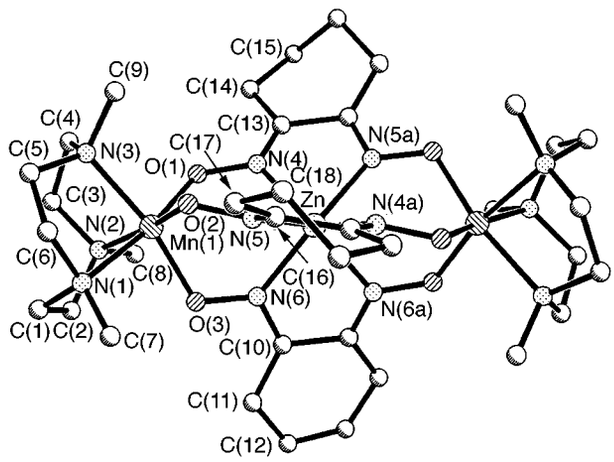

Fig. 2 An ORTEP[11] view of the trinuclear $Mn^{IV}Zn^{II}Mn^{IV}$ cation in complex **4**

Analyses of the cyclic voltammograms in the more negative potential range (0.0 to −1.0 V) with varying scan rates revealed two additional quasi-reversible reduction steps attributable to the equilibria $Mn^{III}M^{II}Mn^{III} \overset{Red_1}{\rightleftharpoons} Mn^{II}M^{II}Mn^{III} \overset{Red_2}{\rightleftharpoons} Mn^{II}M^{II}Mn^{II}$. Identical cyclic voltammetric behaviour has been observed for complexes **4**–**6**. All attempts to isolate the mixed-valence complexes of $Mn^{IV}M^{II}Mn^{III}$ or $Mn^{III}M^{II}M^{II}$ proved to be unsuccessful, presumably due to the low comproportionation constant K_c for the equilibrium, *e.g.*, $Mn^{III}M^{II}Mn^{III} + Mn^{IV}M^{II}Mn^{IV} \overset{K_c}{\rightleftharpoons} 2\ Mn^{IV}M^{II}Mn^{III}$.

Structures of $Mn^{IV}Zn^{II}Mn^{IV}$ 4 and $Mn^{IV}Cu^{II}Mn^{IV}$ 5

Although the analytical and spectroscopic data unambiguously showed the presence of the trinuclear MnZnMn and MnCuMn cores as the smallest unit in the cation, X-ray analyses were undertaken to remove the doubts regarding connectivity. Unfortunately severe disorders of the solvent molecule, the bridging ligand and of the central copper were main obstructions to good-quality structure determinations, particularly for complex **5**. Nevertheless, in spite of the high *R* factors and large standard deviations due to unsatisfactory refinements, the crystal structure analyses of **4** and **5** confirmed their heterotrinuclear nature with Mn^{IV} as the terminal ions.

The molecular geometry and the atom labelling scheme of the cation in complex **4** are shown in Fig. 2. The structure of the complex cation consists of a discrete tetracationic trinuclear unit having a crystallographic two-fold symmetry, and four non-co-ordinatively bound perchlorate anions. Selected bond lengths and angles are listed in Table 3. The structure confirms that a linear trinuclear complex, Mn(1)–Zn(1)–Mn(1a) 179.9°, has indeed been formed in such a way that a trioctahedral

Table 2 Crystal data for $[L_2Mn^{IV}{}_2(niox)_3Zn][ClO_4]_4\cdot 2MeCN$ **4**

Formula	$C_{40}H_{72}Cl_4Mn_2N_{14}O_{22}Zn$
M	1418.2
Crystal size/mm	0.30 × 0.28 × 0.42
Colour, habit	Black prism
Crystal system	Monoclinic
Space group	$C2/c$
a/Å	30.06(4)
b/Å	9.659(12)
c/Å	22.42(3)
β/°	113.66(10)
U/Å^3	5964(13)
Z	4
D_c/g cm^{-3}	1.534
μ/mm^{-1}	1.077
F(000)	2848
Number of independent reflections	5218
Number of observed reflections	2727 [$F > 2\sigma(F)$]
Number of parameters refined	396
Data-to-parameter ratio	6.9 : 1
Weighting scheme, w^{-1}	$\sigma^2(F) + 0.0020F^2$
R,[a] R' [b]	0.0955, 0.1193

[a] $R = \Sigma||F_o| - |F_c||/\Sigma|F_o|$. [b] $R' = [\Sigma w(|F_o| - |F_c|)^2/\Sigma w|F_o|^2]^{\frac{1}{2}}$.

Table 3 Selected bond lengths (Å) and angles (°) for $[L_2Mn^{IV}{}_2(niox)_3Zn][ClO_4]_4\cdot 2MeCN$ **4**

Mn(1)···Zn	3.49	Mn(1)···Mn(1a)	6.97
Zn–N(4)	2.081(10)		
Zn–N(6)	2.105(11)	Zn–N(5)	2.086(14)
Mn(1)–O(1)	1.882(12)	Mn(1)–O(2)	1.887(8)
Mn(1)–O(3)	1.888(9)	Mn(1)–N(1)	2.089(15)
Mn(1)–N(2)	2.074(10)	Mn(1)–N(3)	2.079(10)
O(1)–N(4)	1.367(14)	O(2)–N(5)	1.351(14)
O(3)–N(6)	1.357(16)	N(5)–C(16)	1.247(16)
N(4)–C(13)	1.263(22)	N(6)–C(10)	1.287(16)
C(10)–C(10a)	1.495(31)	C(13)–C(14)	1.509(18)
C(13)–C(13a)	1.519(20)	C(14)–C(15)	1.561(30)
C(10)–C(11)	1.472(20)	C(16)–C(17)	1.512(25)
C(11)–C(12)	1.453(26)	C(17)–C(18)	1.513(21)
N(4)–Zn–N(5)	87.4(4)	N(4)–Zn–N(6)	87.2(4)
N(5)–Zn–N(6)	87.5(5)	N(4)–Zn–N(4a)	137.2(6)
N(4)–Zn–N(5a)	74.4(4)	N(5)–Zn–N(5a)	129.2(6)
N(6)–Zn–N(5a)	136.8(5)	N(6)–Zn–N(6a)	74.3(6)
N(4)–Zn–N(6a)	129.1(4)		
Mn(1)–Zn–Mn(1a)	179.9	O(1)–Mn(1)–O(2)	98.8(4)
O(1)–Mn(1)–O(3)	98.9(5)	O(2)–Mn(1)–O(3)	99.2(4)
O(1)–Mn(1)–N(1)	169.4(4)	O(2)–Mn(1)–N(1)	87.7(5)
O(3)–Mn(1)–N(1)	88.1(5)	O(1)–Mn(1)–N(2)	89.7(5)
O(2)–Mn(1)–N(2)	168.8(5)	O(3)–Mn(1)–N(2)	86.5(4)
N(1)–Mn(1)–N(2)	82.8(5)	O(1)–Mn(1)–N(3)	87.5(5)
O(2)–Mn(1)–N(3)	88.6(4)	O(3)–Mn(1)–N(3)	169.0(4)
N(1)–Mn(1)–N(3)	84.4(5)	N(2)–Mn(1)–N(3)	84.6(4)
Mn(1)–O(1)–N(4)	117.0(7)	Mn(1)–O(2)–N(5)	117.0(8)
Mn(1)–O(3)–N(6)	117.3(7)		
Zn–N(4)–C(13)	118.3(9)	Zn–N(4)–O(1)	124.5(8)
Zn–N(5)–O(2)	124.6(8)		
Zn–N(5)–C(16)	119.3(11)	Zn–N(6)–C(10)	118.5(9)
Zn–N(6)–O(3)	123.9(7)		

geometry containing a zinc(II) and two manganese(IV) as central atoms is present in the lattice. The central tris(nioximato)-zincate(II) ion, $[Zn(niox)_3]^{4-}$, bridges the two terminal manganese(IV) centres through the deprotonated oxime oxygens, O(1), O(2) and O(3). The terminal manganese co-ordination geometry is distorted octahedral with three nitrogen atoms from the facially co-ordinated tridentate macrocyclic amine and three oxygen atoms from three bridging oximate groups. The central ZnN_6 core is nearly trigonal prismatic. The six azomethine nitrogens are arranged around the zinc(II) centre with a twist angle of 5.5° between the triangular faces comprising N(4)N(5)N(6) and N(4a)N(5a)N(6a) atoms. In other words, the co-ordination polyhedron around Zn(1) is 54.5° away from the

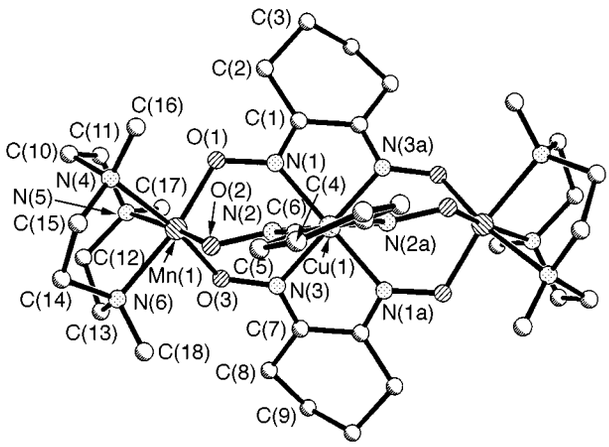

Fig. 3 Structure of the tetracation $Mn^{IV}Cu^{II}Mn^{IV}$ in complex **5**

octahedral geometry. An intramolecular Mn(1)···Mn(1a) separation of 6.97 Å has been found. The nearest-neighbour Mn(1)···Zn(1) distance within the trinuclear cation of 3.49 Å is slightly shorter than that in the corresponding $Mn^{III}Zn^{II}Mn^{III}$ compound with dimethylglyoxime[2] as the bridging ligand. The average Zn–N distance of 2.091(12) Å is not significantly different within the 3σ criterion from that in similar trinuclear M_tZnM_t complexes.[12] The average Mn^{IV}–N 2.081(12) and Mn^{IV}–O 1.886(10) Å bond lengths are similar to those found earlier[13] and are slightly shorter, as expected, than those in the analogous manganese(III) compounds.[2] The bond lengths are consistent with a d^3 electron configuration of the terminal manganese(IV) centres.

As the structure of complex **5** is not up to normal crystallographic standards with $R_1 = 0.1184$, we are refraining from publishing the crystal data§ in detail. However, the atom connectivities together with the heterotrinuclear nature with Mn^{IV} as the terminal ions are clear even at the present state of refinement. The cyclohexyl rings show conformational disorder with unreasonably large apparent thermal parameters of the outwardmost methylene carbon atoms. This is probably due to the presence of two half-chair conformations. As in the case of **4**, perchlorate anions and acetonitrile molecules are also disordered in **5**. Copper had to be refined with a split model. The occupancy factors are $K = \frac{1}{3}$ and $\frac{1}{6}$ (on a two-fold axis) for the asymmetric unit giving three equivalent copper positions for the cation. The structure of **5** consists of distinct $[L_2Mn^{IV}{}_2(niox)_3Cu]^{4+}$ cations and non-co-ordinatively bound perchlorate anions (Fig. 3). The central Cu is six-co-ordinated by azomethine nitrogen atoms of the three nioxime ligands. The $[Cu(niox)_3]^{4-}$ anion bridges two terminal manganese(IV) ions through its deprotonated oxime oxygens with a Mn···Cu separation of 3.54 Å. The trinuclear Mn–Cu–Mn unit is not perfectly linear with an angle of 171° and the Mn···Mn separation is 7.06 Å. The co-ordination geometry of the terminal manganese ions is distorted octahedral with three nitrogen atoms from the facially co-ordinated tridentate macrocyclic amine (L) and three oxygen atoms from the deprotonated nioxime ligands, resulting in *fac*-MnN_3O_3 chromophores. The Mn–N (average 2.08 Å) and Mn–O (average 1.87 Å) distances are very similar to those in **4** and comparable to literature values for d^3 electron configurations of the terminal manganese(IV) centres.[13]

The Cu–N distances of 2.30, 2.00 and 1.96 Å are different from each other and show together with the twist angles (5.9, 8.4, 8.4°) that the resultant co-ordination sphere around the disordered Cu is strongly distorted. The Cu atom is thus dis-

§ $C_{36}H_{66}Cl_4CuMn_2N_{12}O_{22}\cdot 2CH_3CN$, monoclinic, space group $C2/c$, $a = 30.39(2)$, $b = 9.518(11)$, $c = 22.53(2)$ Å, $\beta = 113.46(6)°$, $U = 5977(9)$ Å^3, $Z = 4$, $R = 0.154$ for 4589 unique observed intensities, $T = 173$ K.

Table 4 Magnetic parameters for trinuclear complexes **1**–**6** containing nioxime as bridging ligand

Compound	J_a/cm^{-1} ($J_{12} = J_{23}$)	J_t/cm^{-1} ($= J_{13}$)	g_{Mn} $g_x = g_y = g_z$	$\|D_{Mn}\|$/cm^{-1} (fixed)	$(E/D)_{Mn}$
1* $Mn^{III}Zn^{II}Mn^{III}$	—	−2.4	1.94	5	—
2* $Mn^{III}Cu^{II}Mn^{III}$	−70	−3.9	1.98	5[a]	0.12
3* $Mn^{III}Mn^{II}Mn^{III}$	4.7	−3.4	1.99	5	—
4 $Mn^{IV}Zn^{II}Mn^{IV}$	—	−20.6	2.02	5	—
5 $Mn^{IV}Cu^{II}Mn^{IV}$	50.1	−17.7	1.94	5	0.16
6 $Mn^{IV}Mn^{II}Mn^{IV}$	25.2	−25.7	2 (fixed)	5	—

[a] $D_{Mn} = -5$ cm^{-1}; sign was determined by field-dependent magnetization measurements (Fig. 7).

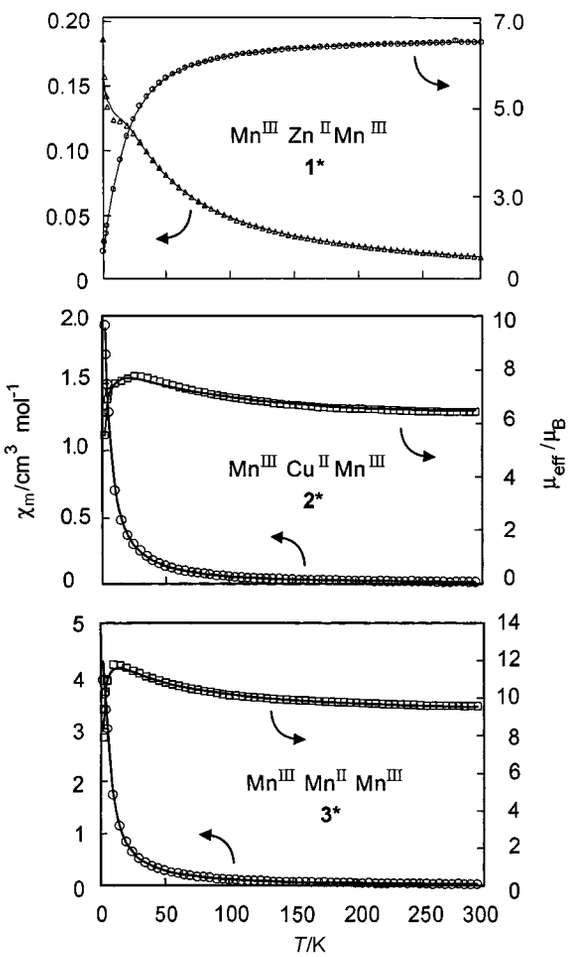

Fig. 4 Temperature dependence of the magnetic susceptibility and moments for complexes **1***–**3***. The solid lines represent the best least-squares fits of the experimental data to the HDvV model

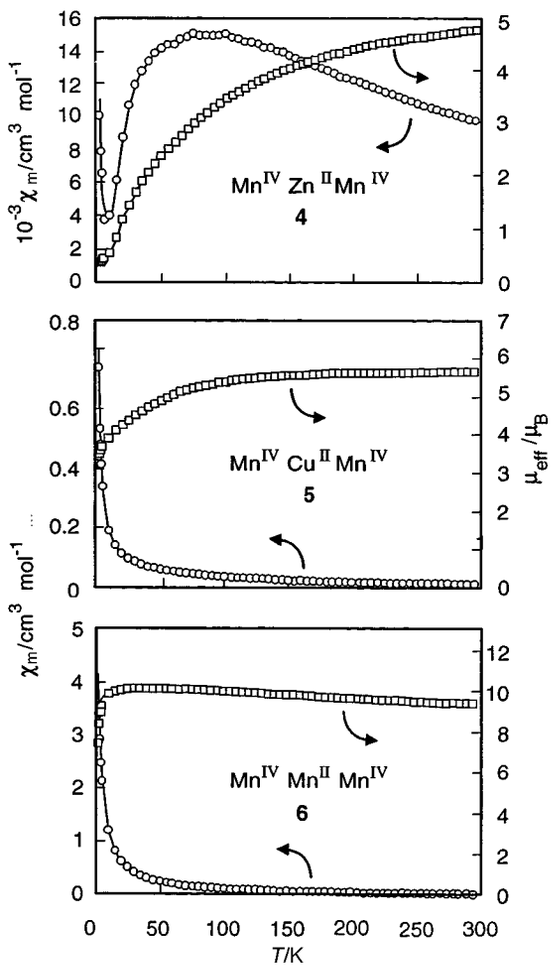

Fig. 5 Thermal dependence of the magnetic moment for complexes **4**–**6**. The solid lines represent the simulation with the spin Hamiltonian $H = -2JS_AS_B$ (see text)

placed from the centre of the complex and more close to two of the bridging nioxime ligands; the distance of the third oxime ligand is remarkably long. The geometry of the copper centre may be envisaged as a pseudo-square pyramid with an η^2-niox ligand at the apical position, and is very similar to that found in the other $M^{III}_2Cu(dmg)_3$ compounds.[1,2]

Magnetic susceptibility and EPR studies

Magnetic susceptibility data for polycrystalline samples of complexes **1**–**6** were collected in the temperature range 2–295 K using a SQUID magnetometer in an applied external magnetic field of 1.0 T. The experimental data, χ_{exptl}, were converted into the molar paramagnetic susceptibility, χ_m, by correcting for underlying diamagnetism, χ_D, which was calculated by use of Pascal's tabulated constants. No temperature-independent paramagnetism χ_{TIP} was considered. The effective magnetic moments, μ_{eff}, as a function of temperature are shown in Figs. 4 and 5.

We use the usual isotropic Heisenberg–Dirac–van Vleck (HDvV) exchange Hamiltonian (1) for three linearly coupled

$$H = -2J_a(S_1S_2 + S_2S_3) - 2J_t(S_1S_3) \quad (1)$$

spins with S_1 and S_3 representing the spins of the terminal metal ions and S_2 that of the central metal ions. In our model $J_a(= J_{12} = J_{23})$ represents the exchange interaction between the 'adjacent' metal ions, whereas J_t describes the interaction between the 'terminal' metal ions, within the trinuclear entity. The experimental magnetic data were simulated using a least-squares fitting computer program with a full-matrix diagonalization approach including exchange coupling, Zeeman splitting, the conventional zero-field interaction (DS_z^2), and a term correcting for an unknown paramagnetic impurity, PI. We have routinely searched for the global nature of the fit minima in the fit–error contour maps for J_a *vs.* J_t to exclude the possible ambiguities of the fit parameters. The solid lines in Figs. 4 and 5 represent the simulations. Table 4 summarizes the intramolecular exchange parameters.

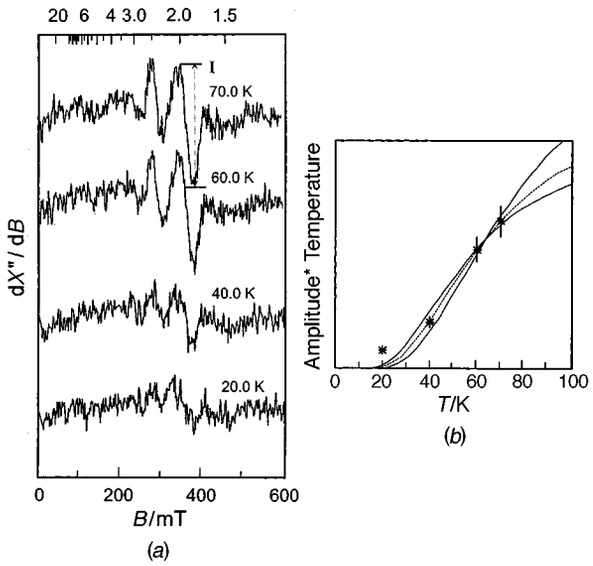

Fig. 6 (*a*) The EPR spectra of complex **4** in MeCN in the temperature range 20–70 K. Conditions: modulation amplitude 1 mT, modulation frequency 100 kHz, microwave power 200 μW, microwave frequency 9.4312 GHz. (*b*) Temperature dependence of the amplitude temperature. Amplitude = peak-to-peak signal at $g \approx 2$. The dashed line is the calculated Boltzmann function for the excited $S_t = 2$ state. The solid lines are the boundary fits

The μ_{eff} values for complex **1*** vary slightly over the temperature range from 6.54 ($\chi_m T = 5.34$) at 295 K to 5.59 μ_B ($\chi_m T = 3.91$ K cm^3 mol^{-1}) at 45 K. Below 45 K the magnetic moment starts to decrease rapidly reaching a value of $\mu_{eff} = 1.72$ μ_B ($\chi_m T = 0.37$ K cm^3 mol^{-1}) at 2 K. The theoretical spin-only value for two uncoupled spins of $S_1 = S_3 = 2$ is 6.93 μ_B, which is slightly higher than the experimental value of 6.54 μ_B at 295 K. Accordingly, a very weak antiferromagnetic coupling $J_t = -2.4$ cm^{-1} with an average $g = 1.94$ and PI($S = 2.5$) = 6.1% have been evaluated through the fitting procedure (Fig. 4).

Interestingly, for complex **4**, the two-electron-oxidation product of **1**, $Mn^{IV}Zn^{II}Mn^{IV}$, a moderately strong antiferromagnetic coupling ($J_t = -20.6$ cm^{-1}) between the terminal manganese(IV) centres ($S_{Mn} = \frac{3}{2}$), separated by a large distance of 6.97 Å, has been observed. The magnetic moment for **4** with $\mu_{eff} = 4.79$ μ_B ($\chi_m T = 2.87$ K cm^3 mol^{-1}) at 295 K decreases steadily reaching a very low value of 0.40 μ_B at 2 K indicating a diamagnetic ground state ($S_t = 0$). The low, but non-negligible residual moment of 0.40 μ_B at 2 K has been attributed to a monomeric ($S = 2$) impurity (≈1%). The plot of χ_m *vs.* T (Fig. 5), exhibiting a broad maximum at ≈75–100 K, is also typical for antiferromagnetically coupled dinuclear complexes. The EPR spectra of **4**, as expected, do not show any resonance below temperature 20 K and thus corroborate the finding of antiferromagnetic coupling between two manganese(IV) centres in **4**. This complex, $Mn^{IV}Zn^{II}Mn^{IV}$, demonstrates the presence of intramolecular antiferromagnetic exchange coupling of considerable magnitude over distances ≈7 Å, indicating that the effective magnetic orbitals are favourably aligned.

The X-band EPR spectra of complex **4**, recorded in the temperature range 20–70 K, are governed by two temperature-dependent signals around $g \approx 2$ (Fig. 6). Its intensity (I) exhibits significant temperature dependence, indicating that the spectra originate from the excited states ($S_t = 1$, 2 or 3) due to $\Delta M_s = \pm 1$ transitions, with a negligible zero-field splitting $|D| \leqslant 0.3$ cm^{-1}. This does not exclude, however, the presence of a local zero-field splitting for Mn^{IV}. Subsequently we plotted IT *versus* T, which to a first-order approximation is proportional to the Boltzmann function of the resonating levels. In this presentation, an isolated spin manifold, obeying a Curie–Weiss law, would yield a horizontal straight line for $T \gg 0.4$ K. A significant temperature dependence of IT is observed, as shown in Fig. 6(*b*). It is difficult to determine the intensity of the signal at 20 K, because of its noisy nature and hence the EPR signal around $g \approx 2$ at 20 K has not been considered for the simulation shown in Fig. 6(*b*). The fading below 20 K and the strong rise at elevated temperatures demonstrate that the spectra originate from excited states and that the ground state is diamagnetic and EPR silent, in accordance with the susceptibility findings.

For quantitative analysis we compared the experimental data IT with theoretical Boltzmann functions, derived from the spin-coupling model for two spins of $S = \frac{3}{2}$. Best agreement was obtained with the function describing the thermal population of the excited quintet state $S_t = 2$, equation (2), where

$$I(S_t = 2)\cdot T \propto \exp(6J/kT)/z \qquad (2)$$

$z = 1 + 3\exp(2J/kT) + 5\exp(6J/kT) + 7\exp(12J/kT)$. The dotted line in Fig. 6(*b*) is a fit with $J = -16.5$ cm^{-1} with an estimated error (solid lines) of ±3.5 cm^{-1}. This is in agreement with the exchange coupling constant of $J_t \approx -20$ cm^{-1}, evaluated from the susceptibility analysis. Hence, we assign the EPR spectrum to the excited state $S_t = 2$ of complex **4**. The EPR spectrum of **4** in MeCN solution also demonstrates unambiguously the intramolecular nature of the exchange interaction.

The magnetic moment for $Mn^{III}Cu^{II}Mn^{III}$ **2*** increases from 6.42 μ_B ($\chi_m T = 5.16$ K cm^3 mol^{-1}) at 295 K as the temperature is lowered until a maximum is reached at ≈25 K with $\mu_{eff} = 7.76$ μ_B ($\chi_m T = 7.54$ K cm^3 mol^{-1}) (Fig. 4), which is close to the spin-only value of $\mu_{eff} = 7.94$ μ_B for $S = \frac{7}{2}$. Below 25 K there is a decrease in μ_{eff} reaching a value of 5.57 μ_B ($\chi_m T = 3.88$ K cm^3 mol^{-1}) at 2 K. The magnetism of **2*** can be interpreted in terms of an antiferromagnetic coupling between the neighbouring high-spin manganese(III) ($S_{Mn} = 2$) and copper(II) ion ($S_{Cu} = \frac{1}{2}$) and between the terminal manganese(III) ions, yielding an irregular spin-state structure[14] with $S_t = \frac{7}{2}$ ground state. Simulation for **2*** using the HDvV model yielded antiferromagnetic coupling constants $J_a = -70.0$ cm^{-1} and $J_t = -3.9$ cm^{-1} with $g_{Mn} = 1.98$ and $g_{Cu} = 2.1$ (fixed). To fit particularly the low-temperature data it is necessary to consider the zero-field splitting parameter for Mn^{III}, D_{Mn}, which was held constant during the fitting procedure. It is important to note that the simulations of μ_{eff} are not very sensitive to the sign of D_{Mn} and it is difficult, if not impossible, to determine unambiguously this sign from powder magnetic susceptibility measurements. A fixed value of $|D_{Mn}|$ at 5.0 cm^{-1} was found to be best suited for the simulation. The solid line in Fig. 4 is the theoretical curve obtained with the parameters listed in Table 4. Local g_{Mn} dominates over local g_{Cu} as can be seen in the molecular g-tensor expressions (3) and (4)[15–17] in determining the g values of the

$$g_{|\frac{7}{2},4\rangle} = \tfrac{10}{9}\, g_{Mn} - \tfrac{1}{9}\, g_{Cu} \qquad (3)$$

$$g_{|\frac{5}{2},3\rangle} = \tfrac{8}{7}\, g_{Mn} - \tfrac{1}{7}\, g_{Cu} \qquad (4)$$

low-lying states in complex **2***. The first excited state with an $S_t = \frac{5}{2}$ lies about 40 cm^{-1} higher in energy than the ground state of $S_t = \frac{7}{2}$. A similar behaviour has been observed for the analogous $Mn^{III}Cu^{II}Mn^{III}$ and related $Fe^{III}Cu^{II}Fe^{III}$ compounds with dimethylglyoximate[1,2] ligands. The energy scheme obtained from the susceptibility data for **2*** is further verified by isothermal magnetization measurements at 5 K and up to 5 T. The data are given as triangles in Fig. 7. The solid line represents the theoretical magnetization behaviour with the parameters $J_a = -70.0$ cm^{-1}, $J_t = -3.86$ cm^{-1}, $g_{Mn} = 1.98$, $g_{Cu} = 2.1$, $D_{Mn} = -5.0$ cm^{-1}, $(E/D)_{Mn} = 0.12$. The agreement between the calculation and the experimental data is very good. This clearly shows that the lowest-lying state is $S_t = \frac{7}{2}$ and corroborates with the data deduced from the magnetic susceptibility measurement (Fig. 4). It must be pointed out that the fit in Fig. 7 could not be obtained with $D_{Mn} = +5$ cm^{-1}. Remarkably, contrary to **2***, the coupling between manganese(III) and copper(II) ions in oxime-

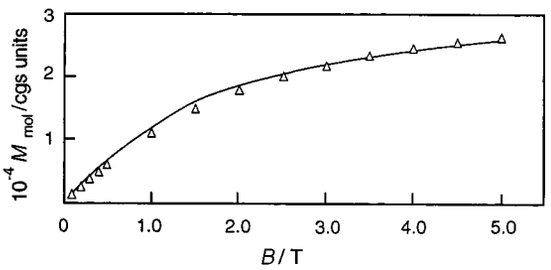

Fig. 7 Field-dependent magnetization for complex **2***. The solid line is the simulation with the parameters given in the text

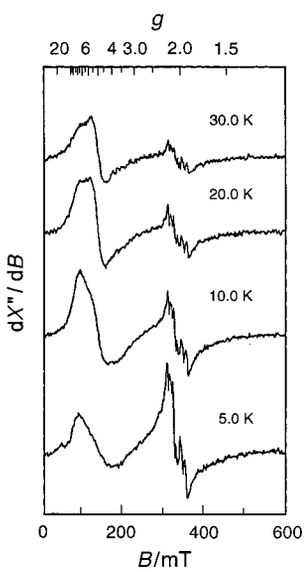

Fig. 8 The EPR spectra of complex **2*** in MeOH in the temperature range 5–30 K. Conditions: modulation amplitude 1 mT, modulation frequency 100 kHz, microwave power 200 μW, microwave frequency 9.4319 GHz

bridged compounds described in the literature[18,19] so far is ferromagnetic in nature.

Fig. 8 shows the EPR spectra in MeOH for complex **2*** in the temperature range 5.0–30.0 K. The spectrum at 5 K shows a broad signal passing through zero intensity at an effective value of $g \approx 5$. This signal can be readily simulated by adopting spin $S_t = \frac{7}{2}$ and effective g values of $g_y = 4.9(1)$, $g_x = 5.0(1)$, $g_z = 4.9(1)$ and can be assigned to the $|S_t = \frac{7}{2}; m_{st} = \pm\frac{3}{2}\rangle$ Kramers doublet with rhombicity $(E/D)_{\frac{7}{2}} = 0.12(1)$. Associated with this assignment is the condition $|D_{\frac{7}{2}}| \gg h\nu \approx 0.3$ cm^{-1} (for X-band EPR); the local zero-field splitting D_{Mn} is hence different from zero due to the relation (5). This is in line with the value $D_{Mn} = -5$

$$|D_{|\frac{7}{2},4\rangle}| = \tfrac{11}{21}|D_{Mn}| \qquad (5)$$

cm^{-1} derived from the magnetization measurements (Fig. 7). Thus the ground-state $S_t = \frac{7}{2}$ for **2*** found by magnetic measurements is corroborated by the X-band EPR spectra. The high rhombicity may be due to the strong distortion of the copper(II) centre owing to the Jahn–Teller effect. The six-line signal in the EPR spectra (Fig. 8) at $g \approx 2$ with a shoulder at $g \approx 2.1$, the intensity of which decreases with increasing temperature, has been assigned to the overlap of two different signals, one originating from copper(II) ($S_{Cu} = \frac{1}{2}$) impurities, and the other from the hyperfine structure of manganese(II) ($S_{Mn} = \frac{5}{2}$, $I_{Mn} = \frac{5}{2}$) impurities.

Interestingly, the μ_{eff} value of 5.66 μ_B ($\chi_m T = 4.0$ K cm^3 mol^{-1}) at 295 K decreases monotonically to $\mu_{eff} = 3.44$ μ_B ($\chi_m T = 1.48$ K cm^3 mol^{-1}) at 2 K for complex **5**, $Mn^{IV}Cu^{II}Mn^{IV}$, which is slightly smaller than the spin-only value of $\mu_{eff} = 3.87$ μ_B for $S = \frac{3}{2}$. An excellent fit (Fig. 5) of the magnetic data employing the HDvV model ($S_1 = S_3 = S_{Mn} = \frac{3}{2}$, $S_2 = S_{Cu} = \frac{1}{2}$)

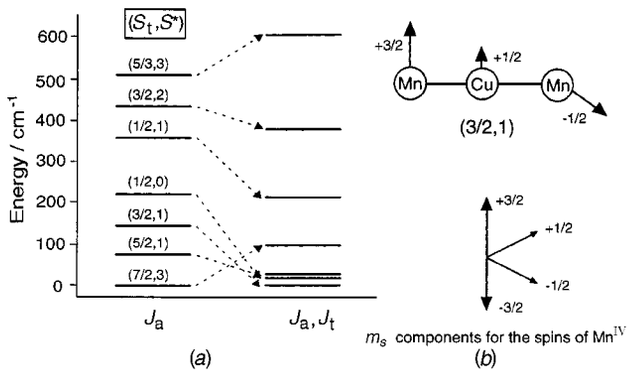

Fig. 9 (*a*) Spin ladder for complex **5** with (right) and without (left) J_t. (*b*) Orientation of the spins for the ground state $S_t = \frac{3}{2}$

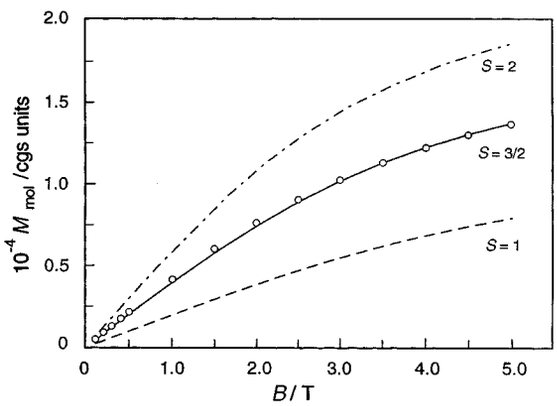

Fig. 10 Plot of magnetization (○) *versus* the applied magnetic field for complex **5**. The solid line represents the Brillouin function for $S = \frac{3}{2}$ with $g = 2.06$. The dashed lines represent the theoretical magnetization curves for $S = 1$ and 2 with $g = 2.00$

yields $J_a = +50.1$ cm^{-1}, $J_t = -17.7$ cm^{-1}, $g_{Mn} = 1.94$, $g_{Cu} = 2.1$ (fixed), $D_{Mn} = 5.0$ cm^{-1} (fixed), $(E/D)_{Mn} = 0.16$. The nearest-neighbour coupling, *i.e.* the exchange interaction between manganese(IV) and copper(II) ions, J_a, is ferromagnetic in nature, but the spin interaction between the terminal manganese(IV) ions is antiferromagnetic with $J_t \approx -18$ cm^{-1}. This relatively strong coupling, considering the long distance of 7.06 Å between the terminal manganese centres, has a profound influence on the structure of the spin ladder yielding a ground state with $S_t = \frac{3}{2}$ for **5**, which lies 14.6 cm^{-1} below the first excited state with $S_t = \frac{1}{2}$ and 20.9 cm^{-1} below the second excited state with $S_t = \frac{5}{2}$. Reducing J_t by 1.25 cm^{-1} would reverse the positions of $S_t = \frac{1}{2}$ and $\frac{5}{2}$, the ground state still being $S_t = \frac{3}{2}$. Neglecting the terminal coupling the ground state of **5** would be $S_t = \frac{7}{2}$. The situation is depicted in Fig. 9. Completely parallel alignment of the spins leading to $S_t = \frac{7}{2}$ is inhibited by the competing antiferromagnetic coupling between the terminal manganese(IV) centres. The g factor for the ground state $S_t = \frac{3}{2}$ is related to the local values g_{Mn} and g_{Cu} by equation (6), indicating the domi-

$$g_{|\frac{3}{2},1\rangle} = \tfrac{2}{3}g_{Mn} + \tfrac{1}{3}g_{Cu} \qquad (6)$$

nance of g_{Mn} over g_{Cu}.

The ground state $S_t = \frac{3}{2}$ obtained from the susceptibility data is further verified by the isothermal magnetization measurements at 5 K in applied fields up to 5 T. The data as circles are shown in Fig. 10. The solid line represents the theoretical magnetization behaviour for $S = \frac{3}{2}$ with $g = 2.06$ and is calculated from expression (7) where $B_s(\chi)$ is the Brillouin function[14] for a

$$M = Ng\mu_B S B_s(\chi) \qquad (7)$$

state S. The dashed lines in Fig. 10 represent the theoretical magnetization curves for $S = 1$ and 2. Fig. 10 clearly shows that

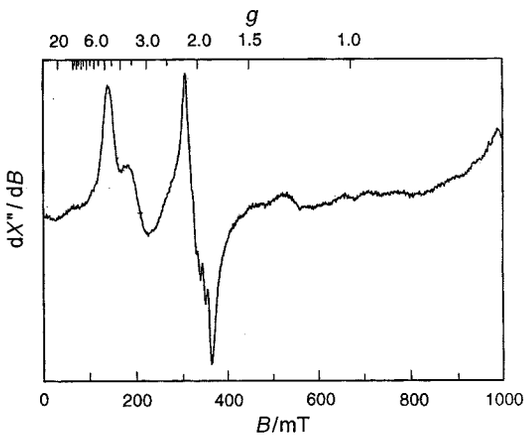

Fig. 11 The EPR spectrum of complex **5** in MeCN at 10 K. Conditions: modulation amplitude 1 mT, microwave power 200 μW, modulation frequency 100 kHz, microwave frequency 9.4236 GHz

the lowest-lying state for **5** is $S_t = \frac{3}{2}$, owing its origin to the two competing exchange interactions J_a and J_t. The magnetic behaviour of **5** is very similar to that of the previously reported analogous $Mn^{IV}Cu^{II}Mn^{IV}$ compound with dimethylglyoxime[2] as the bridging ligand.

The X-band EPR spectrum (Fig. 11) of complex **5** in MeCN at 10 K also confirms the $S_t = \frac{3}{2}$ ground state. The rhombic signal with effective g values of $g_y = 4.8$, $g_x = 3.1$ and $g_z = 1.9$ can be assigned to the $|S_t = \frac{3}{2}, m_{st} = \pm\frac{1}{2}\rangle$ Kramers doublet with a rhombicity $(E/D)_{\frac{3}{2}} = 0.16$. Like **2**, the zero-field splitting in **5** is not negligible ($|D_{\frac{3}{2}}| \gg 0.3$ cm^{-1}) and therefore the local zero-field splitting parameter D_{Mn}, related to $D_{\frac{3}{2}}$ by equation (8), is also

$$D_{|\frac{3}{2},1\rangle} = -\frac{4}{5}D_{Mn} \quad (8)$$

different from zero in qualitative agreement with the finding from magnetic measurements. The strong signal at $g \approx 2.1$ has been assigned to a monomeric copper(II) impurity. It is noteworthy that $E/D \approx 0.16$ for **5** is comparable to that for **2***, $Mn^{III}Cu^{II}Mn^{III}$.

The magnetic behaviour of complex **3***, $Mn^{III}Mn^{II}Mn^{III}$ (Fig. 4), is quite characteristic of a ferromagnetic coupling. At 295 K the μ_{eff} value is 9.57 μ_B ($\chi_m T = 11.45$ K cm^3 mol^{-1}), which is much higher than the value $\mu_{eff} = 9.11$ μ_B ($\chi_m T = 10.37$ K cm^3 mol^{-1}), expected for three non-interacting spins of $S_1 = S_3 = 2$ and $S_2 = \frac{5}{2}$. On lowering the temperature μ_{eff} increases steadily until it reaches at 10 K a value of 11.79 μ_B, which is not far away from the 'spin-only' value of $\mu_{eff} = 11.90$ μ_B for $S = \frac{11}{2}$. Below 10 K there is a rapid decrease in μ_{eff} to 7.93 μ_B ($\chi_m T = 7.86$ K cm^3 mol^{-1}) at 2 K, probably because of the zero-field splitting of the ground state and/or antiferromagnetic intermolecular spin coupling. The fit for complex **3*** by the HDvV model yielded parallel spin coupling between the neighbouring manganese-(III) and -(II) ions with $J_a = +4.7$ cm^{-1} and antiparallel coupling, $J_t = -3.4$ cm^{-1}, between the terminal manganese(III) centres and $g_{Mn^{III}} = 1.99$ and $g_{Mn^{II}} = 2.0$. To fit the low-temperature ($T < 10$ K) data it was necessary to consider the axial zero-field splitting parameter D_{Mn}, which was held constant at 5.0 cm^{-1} during the fitting procedure. With $D_{Mn} = -5$ cm^{-1} (fixed) a fit of poorer quality than that with positive D was obtained. Owing to the competing influence of J_a and J_t upon spin coupling in **3***, the ground state has $S_t = \frac{11}{2}$, and lies 3.1 cm^{-1} below the first excited state with $S_t = \frac{9}{2}$ and 3.7 cm^{-1} below the second excited state with $S_t = \frac{13}{2}$. Neglecting the terminal coupling J_t, the ground state of **3*** would be $S_t = \frac{13}{2}$. Similar ground-state variability, *i.e.* the influence of J_t on the spin ladder, has been unambiguously demonstrated earlier by us.[2] It is known[14,20–23] that the ground state is determined not by the absolute values of J_a and J_t but by their quotient J_t/J_a, which is −0.723 for **3***. We would like to mention here that on replacing nioxime by dimethylglyoxime in

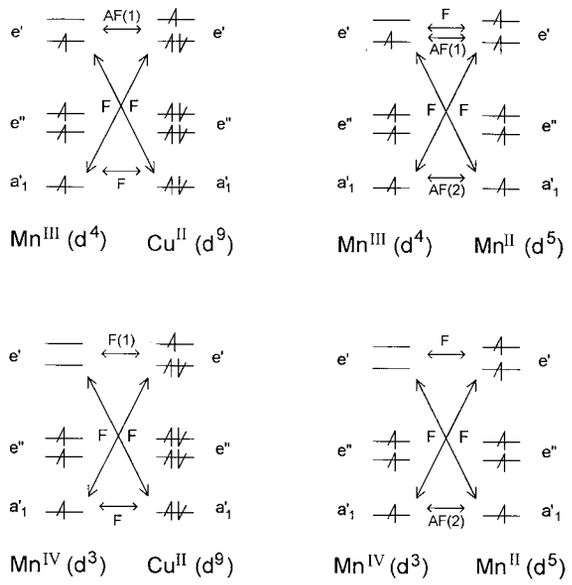

Scheme 1

the corresponding $Mn^{III}Mn^{II}Mn^{III}$ complex the exchange coupling constants of $J_a = +4.7$ cm^{-1}, $J_t = -2.95$ cm^{-1} lead to $J_t/J_a = -0.628$ and as a result the lowest-lying states $S_t = \frac{11}{2}$ and $\frac{13}{2}$ are degenerate for the $Mn^{III}Mn^{II}Mn^{III}$(dmg) complex.[2] It is interesting that the structurally characterized[24,25] linear trinuclear mixed-valence compounds, $Mn^{III}Mn^{II}Mn^{III}$, exhibit antiferromagnetism between the adjacent manganese-(III) and -(II) centres. A very weak ferromagnetic coupling ($J = +0.86$ cm^{-1}) has been observed for a dinuclear $Mn^{III}Mn^{II}$ compound.[26]

The μ_{eff} values for complex **6**, $Mn^{IV}Mn^{II}Mn^{IV}$, increase from $\mu_{eff} = 9.38$ μ_B ($\chi_m T = 11.0$ K cm^3 mol^{-1}) at 295 K slowly to 10.10 μ_B ($\chi_m T = 12.75$ K cm^3 mol^{-1}) at 45 K and below 45 K it starts to decrease steadily reaching a value of $\mu_{eff} = 7.37$ μ_B ($\chi_m T = 6.79$ K cm^3 mol^{-1}) at 2 K (Fig. 5). The parameters used for the least-squares fitting of the experimental data are $J_a = +25.2$ cm^{-1}, $J_t = -25.7$ cm^{-1}, $g_{Mn^{IV}} = g_{Mn^{II}} = 2.0$ (fixed), $D_{Mn^{IV}} = \pm 5$ cm^{-1} (fixed). The quotient J_t/J_a of −1.02 results in the stabilization of the $S_t = \frac{9}{2}$ ground state, which is 23.3 cm^{-1} below the first excited state of $\frac{7}{2}$. In the case of the corresponding $Mn^{IV}Mn^{II}Mn^{IV}$(dmg) complex[2] the ground state of $S_t = \frac{9}{2}$ is also well separated ($\Delta E = 17.2$ cm^{-1}) from the $S_t = \frac{7}{2}$ state.

Conclusion

A qualitative rationale for the trend and the nature of the exchange interactions between the spin carriers can be provided in the framework of the established Goodenough–Kanamori rules[27] for superexchange, as elegantly and clearly outlined in Ginsberg's review.[28]

The evaluated exchange coupling constant consists of two opposing contributions from antiferromagnetic (J_{AF}) and ferromagnetic (J_F) interactions, equation (9), with J_{AF} expressed

$$J = J_{AF} + J_F \quad (9)$$

as a negative term and J_F as a positive term.

We would try to analyse the exchange parameters by considering the idealized sp^2 hybridization of the O and N atoms of the bridging oxime groups, through which the different metal d orbitals interact with each other.[29,30]

The bridge network $Mn(O–N)_3M$ as a whole possesses an idealized D_{3h} symmetry. The five metal d orbitals with the three-fold axis as the axis of quantization (z axis along the Mn···M···Mn vector as the axis of highest symmetry) transform in D_{3h} symmetry as $a_1'(d_{z^2})$, $e''(d_{xz},d_{yz}: t_{2g}$ parentage) and $e'(d_{x^2-y^2}, d_{xy}: e_g$ parentage).

Scheme 1 represents the important exchange pathways oper-

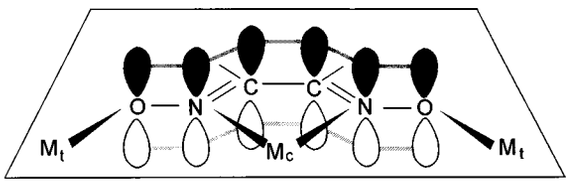

Scheme 2

ating in complexes **2***, **3***, **5** and **6**. It is evident from the antiparallel exchange coupling constant J_a of -70 cm^{-1} for **2*** that the σ-superexchange e′–e′ interaction is dominating the overall spin coupling. Now, on oxidation of Mn^{III} in **2*** to **5** with Mn^{IV}, the singly filled e′ orbitals in **2*** lose the electron making the e′ orbitals at the Mn in **5** completely empty. Thus the antiferromagnetic path AF(1) vanishes. On the other hand, the strong overlap between one empty orbital and one half-filled orbital in **5** yields a moderately strong ferromagnetism, path F(1), thus resulting in an overall ferromagnetic ($J_a = +50.1$ cm^{-1}) spin coupling. The sketched ferromagnetic paths, F, in **2*** (Scheme 1) can be reasonably assumed to provide weak interactions. The same assumption holds equally well for **5**. Thus the drastic change in the nature of the spin coupling, moderate antiferromagnetism to moderate ferromagnetism, on going from Mn^{III} (**2***) to Mn^{IV} (**5**) can be understood on the basis of the presence or absence of an unpaired electron in the e′($d_{x^2-y^2}$, d_{xy}) orbitals.

On going from complex **2***, $Mn^{III}Cu^{II}Mn^{III}$, with the d^4d^9 electronic configuration to **3***, $Mn^{III}Mn^{II}Mn^{III}$, with the d^4d^5 electronic configuration, the sign of the coupling constant reverses to positive, although the strength of the parallel interaction ($J_a = +4.7$ cm^{-1}) is weak. This points out the fact that the antiferromagnetism, AF(1), dominant in **2***, is overcompensated by the presence of several ferromagnetic exchanges, shown as F paths in Scheme 1. As in the case of **5**, with the missing electron in the e′ orbitals, the AF(1) path, present in **3***, vanished, resulting in a stronger parallel coupling in **6** than that in **3***. Along the same lines, the reduction in the ferromagnetic coupling in **6** in comparison to that in **5** can be attributed to the antiferromagnetic path AF(2).

The π-conjugated system of the oxime ligand, delocalized over the whole bridging groups and perpendicular to the plane of the oxime ligand, appears to provide the dominant antiferromagnetic interaction (J_t) between the terminal metal ions, separated by as much as ≈7 Å (Scheme 2). It has been pointed out before[1] that the distortion of the environment of the central metal ion from a trigonal-prismatic arrangement of the ligands toward an octahedron acts as a barrier toward the spin coupling between the terminal metal ions, as a result of the inefficient interaction between the orbitals of the oxime network and the terminal ions. In fact, the terminal spins of $\frac{3}{2}$ in the analogous $Cr^{III}Fe^{II}$(low spin)Cr^{III} (ref. 12) are non-interacting, with the low-spin Fe^{II} exhibiting the greatest twist angle of 34.8°.

Acknowledgements

Our thanks are due to Mrs. M. Hess for technical assistance.

References

1 P. Chaudhuri, M. Winter, B. P. C. Della Védova, P. Fleischhauer, W. Haase, U. Flörke and H.-J. Haupt, *J. Chem. Soc., Chem. Commun.*, 1990, 1728.
2 F. Birkelbach, U. Flörke, H.-J. Haupt, C. Butzlaff, A. X. Trautwein, K. Wieghardt and P. Chaudhuri, unpublished work.
3 K. Wieghardt, P. Chaudhuri, B. Nuber and J. Weiss, *Inorg. Chem.*, 1982, **21**, 3086.
4 J. B. Bush, jun. and H. Finkbeiner, *J. Am. Chem. Soc.*, 1968, **90**, 5903.
5 P. Chaudhuri, M. Winter, B. P. C. Della Védova, E. Bill, A. X. Trautwein, S. Gehring, P. Fleischhauer, B. Nuber and J. Weiss, *Inorg. Chem.*, 1991, **30**, 2148.
6 N. Walker, *Acta Crystallogr., Sect. A*, 1983, **39**, 158.
7 SHELXTL PLUS program package (PC Version), G. M. Sheldrick, Siemens Analytical X-Ray Instruments Inc., Madison, WI, 1990.
8 K. Wieghardt, U. Bossek, D. Ventur and J. Weiss, *J. Chem. Soc., Chem. Commun.*, 1985, 347.
9 R. Blinc and D. Hadzi, *J. Chem. Soc.*, 1958, 4536; K. Burger and F. J. Ruff, *J. Inorg. Nucl. Chem.*, 1965, **27**, 179; J. E. Caton and E. V. Banks, *Inorg. Chem.*, 1967, **6**, 1670.
10 R. S. Nicholson and I. Shain, *Anal. Chem.*, 1964, **36**, 706; A. J. Bard and L. R. Faulkner, *Electrochemical Methods: Fundamentals and Applications*, Wiley, New York, 1980.
11 C. K. Johnson, ORTEP II, Report ORNL 5138, Oak Ridge National Laboratory, Oak Ridge, TN, 1976.
12 D. Burdinski, Diploma Thesis, Bochum, 1995.
13 K. Wieghardt, U. Bossek, B. Nuber, J. Weiss, J. Bonvoisin, M. Corbella, S. E. Vitols and J. J. Girerd, *J. Am. Chem. Soc.*, 1988, **110**, 7398.
14 O. Kahn, *Molecular Magnetism*, VCH, Weinheim, 1993.
15 C. C. Chao, *J. Magn. Reson.*, 1973, **10**, 1.
16 R. P. Scaringe, D. J. Hodgson and W. E. Hatfield, *Mol. Phys.*, 1978, **35**, 701.
17 A. Bencini and D. Gatteschi, *EPR of Exchange Coupled Systems*, Springer, Berlin, 1990.
18 F. Birkelbach, M. Winter, U. Flörke, H.-J. Haupt, C. Butzlaff, M. Lengen, E. Bill, A. X. Trautwein, K. Wieghardt and P. Chaudhuri, *Inorg. Chem.*, 1994, **33**, 3990.
19 F. Lloret, R. Ruiz, M. Julve, J. Faus, Y. Journaux, I. Castro and M. Verdaguer, *Chem. Mater.*, 1992, **4**, 1150.
20 R. L. Martin, in *New Pathways in Inorganic Chemistry*, eds. E. A. V. Ebsworth, A. G. Maddock and A. G. Sharpe, Cambridge University Press, Cambridge, 1968.
21 K. S. Murray, *Adv. Inorg. Chem.*, 1995, **43**, 261; O. Kahn, *Adv. Inorg. Chem.*, 1995, **43**, 179.
22 K. J. Berry, B. Moubaraki, K. S. Murray, P. J. Nichols, L. D. Schulz and B. O. West, *Inorg. Chem.*, 1995, **34**, 4123.
23 D. N. Hendrickson, in *Research Frontiers in Magnetochemistry*, ed. C. J. O'Connor, World Scientific, Singapore, 1993, p. 87.
24 D. P. Kessissoglou, M. L. Kirk, M. S. Lah, X. Li, C. Rapotopoulou, W. E. Hatfield and V. L. Pecoraro, *Inorg. Chem.*, 1992, **31**, 5424.
25 V. Tangoulis, D. A. Malamatari, K. Soulti, V. Stergiou, C. P. Rapotopoulou, A. Terzis, T. A. Kabanos and D. P. Kessissoglou, *Inorg. Chem.*, 1996, **35**, 4974.
26 A. R. Shake, E. A. Schmitt, A. J. Conti, W. E. Streib, J. C. Huffman, D. N. Hendrickson and G. Christou, *Inorg. Chem.*, 1991, **30**, 3192.
27 J. B. Goodenough, *Magnetism and the Chemical Bond*, Wiley, New York, 1963; *J. Phys. Chem. Solids*, 1958, **6**, 287; J. Kanamori, *J. Phys. Chem. Solids*, 1959, **10**, 87.
28 A. P. Ginsberg, *Inorg. Chim. Acta Rev.*, 1971, **5**, 45.
29 T. A. Albright, J. K. Burdett and M. H. Whangbo, *Orbital Interactions in Chemistry*, Wiley, New York, 1985.
30 S. F. A. Kettle, *Symmetry and Structure*, Wiley, Chichester, 1985; R. Krishnamurthy and W. B. Schapp, *J. Chem. Educ.*, 1969, **46**, 799.

Received 7*th July* 1997; *Paper* 7/04771A